Luminescence from ascorbate-stabilized Er$_2$O$_3$ nanoparticles

J. Castañeda-Contreras,[*1] V.F. Marañón-Ruiz[1], M.A. Menéses-Nava[2], R. Chiu Zárate[1], R.A. Rodríguez-Rojas[1],

H. Pérez Ladrón de Guevara[1]

[1]*Centro Universitario de los Lagos, Universidad de Guadalajara, Lagos de Moreno, Jalisco, México*
[2]*Centro de Investigaciones en Óptica, A.C. León, Guanajuato, México*

Abstract—We report a novel method to stabilize Er$_2$O$_3$ nanoparticles with ascorbate ligands. The Er$_2$O$_3$ nanoparticles had strong green and red emissions with sharp and well defined emission peaks. In addition, less intense UV, blue and NIR emissions were also detected. The luminescence was recorded under dynamical pumping at 525nm, 805nm, and 975nm. An enhancement of the red emission is observed when the nanoparticles were pumped at 975nm. We suggest this was due to the absorption cross sections involved in the different pumping schemes.

The optical properties of erbium ions (Er^{3+}) incorporated to solid hosts are of interest, because they provides amplification in the 1550nm communication window [1]. Therefore, Er$_2$O$_3$ is often utilized as a dopant of optical devices such as planar waveguides and fiber amplifiers [2-5]. The main factors involved in the performance of these devices are host phonon energy, OH groups and the clustering of Er$_2$O$_3$. An additional optical feature of Er^{3+} is the NIR to visible up-conversion, which is of interest in applications such as sensors, phosphors and lasers [6]. A well-established strategy to avoid Er$_2$O$_3$ aggregation during the synthesis is by adding coordinating ligands such as citrate [7] or poly-ethylene glycol [8]. The interaction between ligands and lanthanide ions results in a positive charge that prevents aggregation of the species in a solution, i.e. nanosize crystals are obtained [9]. In the present work, Er$_2$O$_3$ nanoparticles were synthesized by a modified co-precipiation method [10], with ascorbic acid as a precursor of stabilizing ligands.

The chemicals were of analytical grade from Sigma-Aldrich Co and utilized as received without any further treatment. The reaction began by dissolving 0.5g of ascorbic acid and 0.0315g of NaF in 10ml of distilled water. Then a solution of 1.25g of erbium nitrate (Er(NO$_3$)$_3$ .6H$_2$O) dissolved in ethanol was added to the NaF-ascorbic acid solution. The resulting mixture was left under continuous stirring for two hours at room temperature, forming a pale pink solution. Subsequently, 15ml of ethanol was added to precipitate the nanoparticles, which were collected by centrifugation. The material in the form of powder was washed twice and dried at room temperature under vacuum. The

* E-mail: jcc050769@gmail.com

nanoparticles were heated in air at 800°C for three hours to remove the ascorbate and promote the Er$_2$O$_3$ crystallization.

X-ray diffraction patterns from our samples (not shown here) were indexed with the JCPDF file 77-0777 for crystalline Er$_2$O$_3$ with a cubic structure. The size of the nanoparticles was calculated by the Scherrer's formula, obtaining an average crystallite size of about 32nm.

TEM images were obtained with a JEOL 4000 transmission electron microscope operating at 3000kV. The TEM micrograph in Fig. 1 shows that most nanoparticles were located in clusters. The nanoparticles had a peak of the size distribution of 40nm, as obtained by the Feret's diameter.

Fig. 1. TEM micrograph of the Er$_2$O$_3$ nanoparticles.

Characteristic up-conversion luminescence from Er^{3+} was recorded when the nanoparticles were irradiated at 805nm and 975nm. In addition, down-conversion luminescence was obtained by pumping the samples at 525nm. A tunable MOPO-SL laser system from Spectra-Physics was utilized as an excitation source. The luminescence from the samples was dispersed with a 0.5m focal length spectrograph Spectra-Pro 500, from Acton-Research. All the measurements were performed at room temperature. An intense green emission was easily observed with the naked eye. Figure 2 shows the recorded spectra, with sharp and well defined emission peaks. The spectra shapes are roughly similar to these

reported by Capobianco [11] for nanosized Y_2O_3 nanocrystals doped with Er^{3+}.

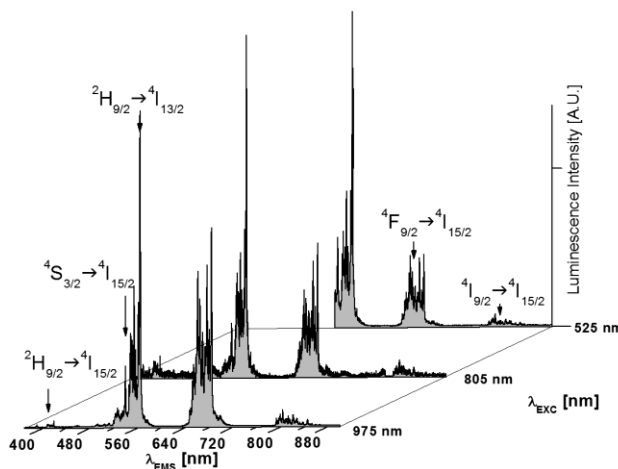Fig. 2. Normalized luminescence spectra from Er_2O_3 nanoparticles pumped at the depicted excitation wavelengths.

The proposed excitation paths for the 525nm excitation wavelength are shown in Fig. 3. There, $^2H_{11/2}$ is populated directly by the pump source. The excited state $^2H_{11/2}$ produced the emission at 530nm and also populated lower-lying $^4S_{3/2}$ by a non–radiative decay. The short $^4S_{3/2}$ lifetime (~1mS on an oxide-based matrix) and the large bandgap to the next lower-lying level promoted a significant decay mechanism through radiative transition $^4S_{3/2}\rightarrow^4I_{15/2}$ at 550nm. On the other hand, the state $^2H_{9/2}$ is populated by a re-absorption of a 550nm photon, and then the 567nm emission is produced from the radiative transition $^2H_{9/2}\rightarrow^4I_{13/2}$ [12]. Successive non-radiative decays populated the lower lying states $^4F_{9/2}$ and $^4I_{9/2}$, giving recorded luminescence at 675nm and 810nm, respectively.

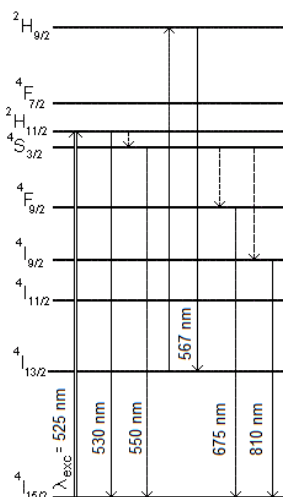

Fig. 3. Simplified energy-levels diagram of Er^{3+} excited at 525nm.

It is well known that up-conversion is produced by mechanisms such as excited state absorption (ESA) and

energy transfer (ET) processes. ESA involves a single ion, and is often related to materials with a low dopant content, while ET usually involves interaction among two or more ions and depends on the dopant content [13]. Therefore, the most probable up-conversion process in our samples was ET, because of the high erbium content in Er_2O_3 [14]. Figure 4a shows the ET processes $(^4I_{9/2}+^4I_{9/2})\rightarrow(^2H_{9/2},^4I_{15/2})$ and $(^4I_{11/2}+^4I_{11/2})\rightarrow(^4F_{7/2}+^4I_{15/2})$, which are promoted by the 805nm and 975nm pump wavelengths, respectively. The re-absorption of a 550nm photon also occurred for the 975nm pump wavelength, as shown in Fig. 4b. The aforementioned description regarding the radiative transitions and non-radiative decays for the excitation at 525nm also applies on these in Fig. 4.
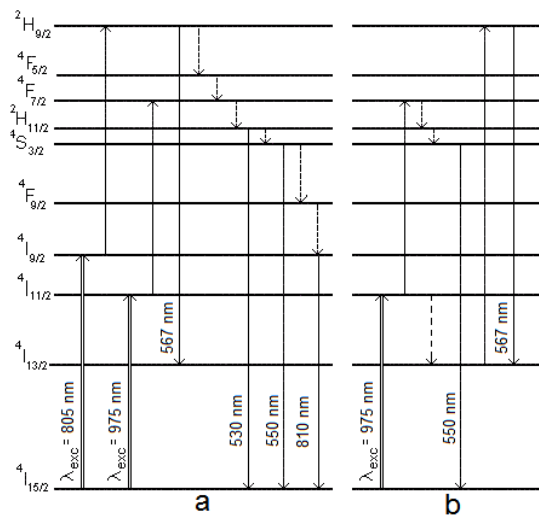

Fig. 4. Simplified energy-levels diagram of Er^{3+} and excitation paths proposed for: (a) the up-conversion emission bands for 805nm and 975nm pump wavelengths, and (b) the re-absorption of a 550nm photon to populate the $^2H_{9/2}$ state.

The spectra in Fig. 2 show a variation of red luminescence upon the pump wavelength: the smallest red emission corresponded to the excitation at 525nm. This is expected as the non-radiative transition $^4S_{3/2}\rightarrow^4F_{9/2}$ involves the emission of several phonons to bridge the energy gap between these excited states, which restrained the red emission to some extent.

The depicted rise of red emissions may be explained in terms of the energy transfer processes (not shown here) that populate the state $^4F_{9/2}$, which are reported so far [11], and to the corresponding cross sections. For the latter, it is reported that the absorption cross section for the process $^4I_{15/2}\rightarrow^4I_{11/2}$ almost doubles the value for $^4I_{15/2}\rightarrow^4I_{9/2}$ [15].

Cross-sections, not calculated here, quantify the ability of an ion to absorb light. Since this behaviour depends strongly on the pump wavelength, we proposed that

population of $^4F_{9/2}$ is favoured at some extent when the Er_2O_3 nanoparticles were irradiated at 975nm.

The spectrum presented in Fig. 5 shows in detail the up-conversion emissions in the blue and UV region from the nanoparticles irradiated at 975nm. A similar behaviour was found for the 805nm pump wavelength. However, we failed to detect these emissions for the excitation at 525nm. The spectrum shows four up-conversion emission bands, these are attributed to the radiative transitions $^4G_{11/2}{\to}^4I_{15/2}$ (390 nm), $^2H_{9/2}{\to}^4I_{15/2}$ (410–420 nm), $^4F_{5/2}{\to}^4I_{15/2}$ (455– 465 nm), and $^4F_{7/2}{\to}^4I_{15/2}$ (483– 510 nm).
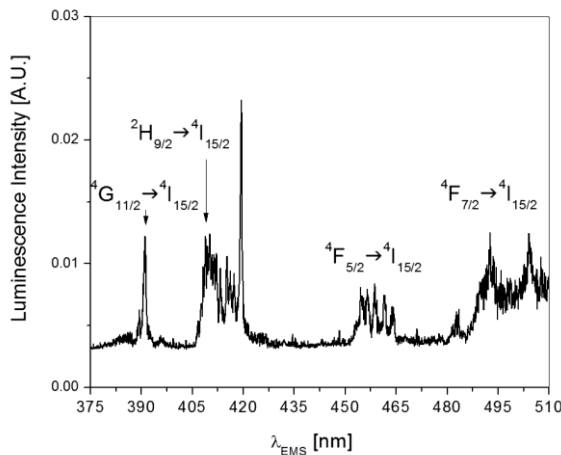

Fig. 5. Blue and UV up-conversion luminescence from Er_2O_3 nanoparticles pumped at 975nm.

Figure 6 shows a probable population path for the state $^2G_{7/2}$ when the samples were pumped at 975nm. As stated before, the $^4F_{7/2}$ state is populated by the ET $(^4I_{11/2}{+}^4I_{11/2}){\to}(^4F_{7/2}{+}^4I_{15/2})$. Afterwards, successive non radiative decays populated $^4S_{3/2}$ state. Then, the ET $(^4S_{3/2}{+}^4I_{11/2}){\to}(^4G_{7/2}{+}^4I_{15/2})$ populated the state $^2G_{7/2}$. From there, multi-phonon relaxations allowed the population of the lower lying states $^4G_{11/2}$, $^2H_{9/2}$, and $^4F_{5/2}$. These gave the depicted luminescence in the UV-blue region.

On the other hand, a proposed mechanism to populate $^2G_{7/2}$ when the samples were irradiated at 805nm is $(^4S_{3/2}{+}^4I_{9/2}){\to}(^2G_{7/2}{+}^4I_{15/2})$. Nevertheless, there is an energy mismatch, which is probably solved by phonons. Work is in progress to clarify this point.
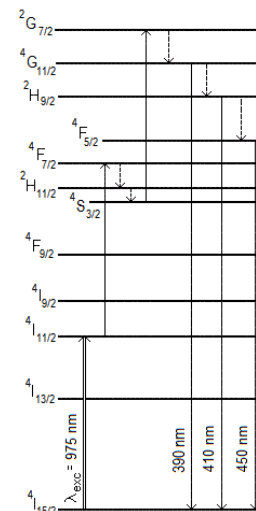

Fig. 6. Excitation path and the corresponding emissions related to $^2G_{11/2}$ excited state under 975nm excitation.

In conclusion, the results show that Er_2O_3 nanoparticles stabilized with ascorbate had strong visible luminescence in the green and red regions. The emissions depended upon the pump wavelength and different population mechanisms.

References

[1] C. Becker, A. Olsson, R. Simpson, *Erbium-Doped Fiber Amplifiers: Fundamentals and Technology* (Boston, Academic Press 1999).
[2] A. Bahtat, M.C. Marco de Lucas, B. Jacquier, B. Varvel, M. Bouazoui. J. Mugnier, J. Opt. Mater. **7**, 173 (1997).
[3] A.J. Kenyon, Progress Quant. Electr. **26**, 225 (2002).
[4] Q. Xiang, Y. Zhou, B.S. Ooi, Y.L. Lam, Y.C. Chan, C.H. Kam, Thin Solid Films **370**, 243 (2000).
[5] L. Zamperdi, M. Ferrari, C. Armellini, F. Visintainer *et al.*, J. Sol-Gel. Sci. Technol. **26**, 103 (2003).
[6] Z. Pan, S.H. Morgan, A. Loper, V. King, B.H. Long, W.E. Collins, J. Appl. Phys. **77**, 4688 (1995).
[7] V. Sudarsan, S. Sivakumar, F.C. van Veggel, Chem. Mater **17**, 4736 (2005).
[8] P.R. Diamente, F.C. van Veggel, J. Fluoresc. **15**, 543 (2005).
[9] K. Lunstroot, L. Baeten, P. Nockemann, J. Martens *et al.*, J. Phys. Chem. C **113**, 15322 (2009).
[10] S. Sivakumar, F.C. van Veggel, S.P. May, J. Am. Chem. Soc. **129**, 620 (2007).
[11] J.A. Capobianco, F. Vetrone, J.C. Boyer, A. Speghini, M. Bettinelly, J. Phys. Chem. B **106**, 1181 (2002).
[12] J. Castañeda, M.A. Menéses-Nava, O. Barbosa, R.A. Rodrıguez, M.V. Félix, Opt. Mat. **21**, 38 (2006).
[13] F. Auzel, Chem. Rev. **104**, 139 (2004).
[14] R. Aghamalyan, J. Contemp. Phys. **44**, 291 (2009).
[15] Y. Choi, K. Kim, J. Am. Ceram. Soc. **82**, 2762 (1999).